FILE COPY

Naval Research Laboratory

Washington, DC 20375-5000

NRL Memorandum Report 6591

AD-A223 189

Computational Investigation of Local Material Strength and Toughness on Crack Growth

V. G. DeGIORGI AND P. MATIC

Mechanics of Materials Branch
Material and Science Technology Division

May 14, 1990

DTIC

Approved for public release; distribution unlimited.

UNCLASSIFIED

SECURITY CLASSIFICATION OF THIS PAGE

REPORT DOCUMENTATION PAGE

Form Approved OMB No. 0704-0188

1a. REPORT SECURITY CLASSIFICATION: UNCLASSIFIED	1b. RESTRICTIVE MARKINGS
2a. SECURITY CLASSIFICATION AUTHORITY	3. DISTRIBUTION / AVAILABILITY OF REPORT: Approved for public release; distribution unlimited.
2b. DECLASSIFICATION / DOWNGRADING SCHEDULE	
4. PERFORMING ORGANIZATION REPORT NUMBER(S): NRL Memorandum Report 6591	5. MONITORING ORGANIZATION REPORT NUMBER(S)
6a. NAME OF PERFORMING ORGANIZATION: Naval Research Laboratory; 6b. OFFICE SYMBOL (If applicable): Code 6382	7a. NAME OF MONITORING ORGANIZATION
6c. ADDRESS (City, State, and ZIP Code): Washington, DC 20375-5000	7b. ADDRESS (City, State, and ZIP Code)
8a. NAME OF FUNDING / SPONSORING ORGANIZATION: Office of Naval Research; 8b. OFFICE SYMBOL (If applicable)	9. PROCUREMENT INSTRUMENT IDENTIFICATION NUMBER
8c. ADDRESS (City, State, and ZIP Code): Arlington, VA 22217	10. SOURCE OF FUNDING NUMBERS: PROGRAM ELEMENT NO. 61153N; PROJECT NO. RR022-01-48; TASK NO.; WORK UNIT ACCESSION NO. DN430-509

11. TITLE (Include Security Classification): Computational Investigation of Local Material Strength and Toughness on Crack Growth

12. PERSONAL AUTHOR(S): DeGiorgi, V. G. and Matic, P.

13a. TYPE OF REPORT	13b. TIME COVERED FROM ____ TO ____	14. DATE OF REPORT (Year, Month, Day)	15. PAGE COUNT
		1990 May 14	50

16. SUPPLEMENTARY NOTATION

17. COSATI CODES: FIELD	GROUP	SUB-GROUP	18. SUBJECT TERMS (Continue on reverse if necessary and identify by block number)
			Crack growth; Finite element; Strain energy

19. ABSTRACT (Continue on reverse if necessary and identify by block number)

Computational simulation of stable crack growth is an important aspect of structural integrity prediction. Modern alloy strength and ductility increase local material fracture toughness but simultaneously complicates stable crack growth predictions. Material modeling, material parameter identification, fracture criterion and numerical crack growth algorithms are issues which must be addressed for robust stable crack growth prediction.

In this investigation, a series of finite element simulations were undertaken to investigate two-dimensional Mode I crack growth in a modified compact (Continued)

20. DISTRIBUTION / AVAILABILITY OF ABSTRACT	21. ABSTRACT SECURITY CLASSIFICATION
☒ UNCLASSIFIED/UNLIMITED ☐ SAME AS RPT ☐ DTIC USERS	UNCLASSIFIED
22a. NAME OF RESPONSIBLE INDIVIDUAL: P. Matic	22b. TELEPHONE (Include Area Code): (202) 767-5215; 22c. OFFICE SYMBOL: Code 6382

DD Form 1473, JUN 86 *Previous editions are obsolete.* S/N 0102-LF-014-6603

SECURITY CLASSIFICATION OF THIS PAGE

UNCLASSIFIED

19. ABSTRACT (Continued)

tension specimen geometry. Two different crack lengths were considered. HY-100 steel parameters, previously characterized for large strain deformation, were utilized. Additional material responses, based on the HY-100 nonlinear response but with different yield strengths and ductilities, were also considered to parametrically assess material effects on crack growth. A debonding algorithm was employed to produce crack growth by nodal release when local material conditions, satisfying a specified local fracture criterion, were met. Material fracture and crack growth were treated as dependent variables of the analysis, generating crack growth in discrete increments.

The results of this parametric computational study demonstrated crack growth of up to sixty-seven percent of the initial crack length over the total number of load increments allowed in each case. The current crack tip energy density histories exhibited piecewise smooth behavior, consistent with the changing crack tip changed position during crack growth. For the materials, geometry, loading and finite element meshes considered, the anticipated load versus displacement discontinuities, corresponding to the discrete crack growth increments, were approximately five percent or less of the current load. The relative loads and crack growth sustained by each specimen were seen to depend on the elastic stress and strain of the material and the local fracture toughness of the material.

CONTENTS

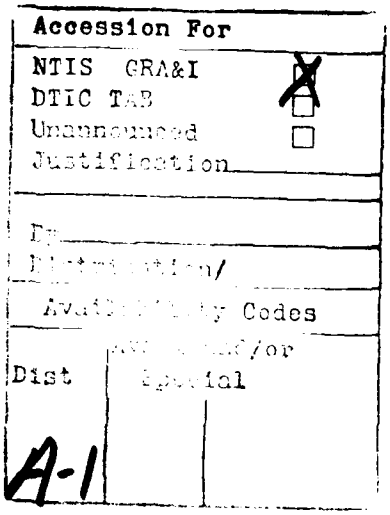

COMPUTATIONAL INVESTIGATION OF LOCAL MATERIAL STRENGTH AND TOUGHNESS ON CRACK GROWTH

I Introduction

Stable crack growth in ductile materials is a fundamentally challenging problem. Material, geometry and load combine to determine fracture tolerance or fracture criticality of a structure. Significant crack growth, if defined as crack growth between minimum detectable crack size and maximum allowable crack size prior to crack instability, may be a large fraction or even many multiples of the minimum detectable crack size. Structures made from modern ductile alloys are, in principle, capable of sustaining such significant crack growth. Prediction of significant crack growth is necessary to determine the rate at which crack instability is approached and if function will be impaired prior to crack instability. Accurate theoretical and computational predictive methodologies are therefore required to develop a fundamental understanding of the crack growth process and to utilize ductile materials effectively for this class of materials.

In this investigation, a typical range of local fracture toughness values are parametrically examined in the context of nonlinear finite element analysis of stable crack growth. A debonding algorithm is employed during the analysis to produce crack growth. The debonding algorithm incorporates a specified local fracture criterion which implements a nodal release scheme to produce crack growth. Material fracture is treated as a dependent variable of the analysis, generating crack growth in discrete increments. These increments satisfy local fracture and equilibrium conditions as imposed by the material, geometry and load. Of particular interest were local material responses at the crack tip, global load versus crack mouth opening displacement and sensitivity of crack growth to material strength and fracture toughness.

II Review of Past Investigations

A wide range of investigations have been performed to examine stable crack growth in ductile materials. Finite element analysis continues to be the major computational technique used for quasistatic ductile material simulation. This is particularly true for materials sustaining large plastic deformation requiring incremental solution. The strong influence of material

Manuscript approved February 2, 1990.

plasticity on the stable crack growth process has been seen in studies of crack behavior in ductile materials. Table 1 summarizes finite element investigations which have addressed stable crack growth problems. Common issues encountered during the modeling process have included (i) the selection of a fracture criterion for use or study, (ii) the material model used, (iii) the material selected, (iv) the cracked specimen geometry and (v) the numerical crack growth scheme. Each of these issues is briefly reviewed. Specific references [1-21] for each issue may be found in Table 1.

Fracture criteria have been postulated on the basis of local, crack tip and global phenomenon. Global approaches were developed as extensions to the energy balance and stability models of elastic fracture. Criteria based on crack tip parameters treat the asymptotic behavior of stress and strain field solutions in the immediate vicinity of the crack tip as the dominant factor in crack growth. Analytically path independent integrals also related the asymptotic field amplitude to far field quantities amenable to common experimental measurements. Local criteria have been developed to explicitly address the various responses a fixed material composition and processing history can exhibit under different local loading conditions.

As fracture criteria address smaller scale phenomenon, the analytical, computational and experimental requirements for implementation increase. The continued and growing interest in local criteria is due, in part, to the wide range of inelastic material responses observed and the cumulative influence such responses have on quasistatic crack growth. The ability to address the necessary requirements to implement such criteria, often theoretically and computationally formidable, are gradually being met.

A number of incremental plasticity models are currently in use. Incremental plasticity models incorporating coupled damage variables have also recieved considerable attention in recent years. (See, for example, the reviews by Chaboche [22], Murakami [23], Nquyen [24] and Sarfarazi [25].) Materials selected for investigation generally reflect a compromise based on relevance, laboratory and testing capabilities, computational capabilities and technical objectives. Consideration of alloys exhibiting extensive ductility, such as effective logarithmic strains of over one hundred

Review of Crack Initiation and Stable Growth Finite Element Modeling

Ref	Author (Date)	Criteria Studied	Mat Model	Material	Geometry	Numerical Crack Growth
[1]	Light, Luxmoore and Evans (1975)	Energy R-Curve	El - Pl	DTD 5020 Al	2D Center Crack 2D Dbl Edge Crack	Node Release
[2]	Light, Luxmoore and Evans (1976)	Energy R-Curve	El - Pl	DTD 5020 Al	2D Center Crack 2D Dbl Edge Crack	Node Release
[3]	Hellan and Lotsberg (1977)	work of separation	El - Pl	---	2D Crack Tip	Node Release
[4]	Nakagaki, Chen and Atluri (1979)	Energy J-Integral CTOA	El - Pl	---	2D Center Crack	Remeshing and Traction Release
[5]	Shih, deLorenzi and Andrews (1979)	J-Integral CTOD	El - Pl	A533B Steel	2D Compact 2D Center Crack	Node release and Spring Elements
[6]	Sorensen (1979)	J-Integral CTOD	El - Perf Pl El - Pl	----	2D Crack Tip	Node Release
[7]	Du and Lee (1982)	----	El - Pl	Al 2024-T3	2D Center Crack	a(t) Node Release
[8]	Du and Lee (1983)	G, COD, COA, J-Integral, stress, strain, energy	El - Pl	Al 2024-T3	2D Center Crack	a(t) Node Release ?
[9]	Carifo, Swedlow and Cho (1986)	J-Integral	El -Pl	7475-T7351 Al	2D Compact	Node Release

[10]	Hoff, Rubin and Hahn (1986)	J-Integral CTOA	El -Pl	A533B Steel	2D Compact	Node Release, Spring and Gap Elements
[11]	Amar and Pineau (1987)	J-Integral weibull stress	El	Low Alloyed Steel	Axi Notched Axi Cracked	Multiple Meshes
[12]	Aoki, Kishimoto, Yoshida and Sakata (1987)	----	El - Pl Void	----	2D Crack Tip with Void	----
[13]	Boone, Wawrzynek and Ingraffea (1987)	stress	Ortho El	Geological	2D Center Crack 2D Dbl Edge Notch 2D Chip Process	Remesh
[14]	Otsuka, Tohgo and Okamoto (1987)	void volume	El - Pl Void	Structural Steel	2D 3-Pt Bend Notch 2D 4-Pt Bend Notch	----
[15]	Miyamoto, Kikuchi,Fujii and Kubo (1987)	J-Integral CTOD	El - Pl Void	Al 7075-T6	2D Crack Tip with voids	---
[16]	Narasimhan and Rosakis (1987)	J-Integral CTOD	El - Perf Pl El - Pl	---	2D Crack Tip	a(t) Node Release
[17]	Shivakumar and Crews (1987)	CTOD Energy	El - Pl	----	2D Compact	Node Release
[18]	DeGiorgi, Kirby and Jolles (1988)	energy J-Integral	El - Pl	HY-100	2D Compact 3D Compact	----
[19]	Kardomateas (1988)	damage	El - Pl	----	Axi Notched	Element Removal
[20]	Zhang and Wang (1988)	COD J-Integral	El - Pl	Structural Steel	3D 3-Pt Bend Notch	----
[21]	Shivakumar and Newman (1989)	CTOD J-Integral	El - Pl	HY-130	2D 3-Pt Bend	Node Release

Notes:

(i) Criteria Studied include crack growth control criteria and quantities examined after crack growth.

(ii) Criteria Studied quantities are upper case if globally based and lower case if locally based.

(iii) Material Models include elastic (El), elastic perfectly-plastic (El - Perf Pl), elastic - plastic (El - Pl), elastic - plastic with void growth parameters (El - Pl Void) and orthotropic elastic (Ortho El).

(iv) Geometries include local crack tip models with asymptotic boundary conditions (Crack Tip, Crack Tip with Voids), panel specimens (Center Crack, Double Edge Crack), compact specimens (Compact), bend specimens (3-Pt Bend Notched, 4-Pt Bend Notched) and axisymmetric specimens (Axi Notched, Axi Cracked)

(v) Numerical Crack Growth generated by an a priori specified crack history denoted by crack length versus time, i.e. a(t), history.

Table 1 Survey of Finite Element Investigations Pertaining to Fracture and Crack Growth

percent, has become possible and increasingly common. Developments in both computational hardware and software have facilitated these investigations. For both types of models, regardless of the specific formulation chosen to describe the inelastic behavior, accurate assessment of material parameters is required for the full range of material response leading to fracture.

Three major approaches have been taken to model crack growth using finite element techniques. These are element removal, remeshing and node release. Each has been used with some success for a variety of different problems. A brief discussion of these techniques is included here.

Element removal, which associates fracture with element stiffness loss, is relatively simple to implement. The effective loss of material at the crack tip significantly alters the crack tip geometry. For materials failing in a diffuse manner, such as concrete, element removal has been successfully used. For metals, however, the crack tip remains relatively distinct. Severe deformation and material separation remain focused at the crack tip throughout crack growth.

Remeshing intermittently recreates the computational model and allocates the necessary resources, in terms of element size and type, to the current critical regions of the model. For linear elastic fracture problems, the process is straightforward. For fracture problems involving incremental plasticity, mesh redefinition accounting for prior material history produces significant computational overhead for the simulation as remeshing occurs. Large gradients also complicate remeshing.

Node release, which generates new surface in a finite element model, remains a popular technique to model fracture. Two element edges, initially constrained to identical displacements, are allowed to separate by releasing the constraints and nodal forces which hold the elements together. Crack surface is formed in a discrete, element by element, succession of node releases. If crack growth is considered as an independent variable for purposes of analysis, the nodal release is provided as a specified nonlinear constraint. If crack growth is not specified a priori but is to be predicted, as is physically the case, a criterion for crack growth must be implemented. The criterion assesses,

on an element by element basis, whether specified conditions for crack growth are satisfied throughout the analysis. If conditions for crack growth are indicated then node release is invoked. In practice, a crack path through the finite element mesh is specified to facilitate implementation and computational efficiency.

III Objectives

In this investigation, the influence of local material behavior on the fracture of ductile materials is addressed. A simple local fracture criterion is implemented, as determined from experimental measurements and computational simulations of material test specimens, relevant to stable crack growth. Crack growth, generated as a result of local material response, was computationally simulated using nonlinear finite element analysis incorporating a debonding algorithm.

With this modeling strategy, a parametric study of debonding sensitivity to material and geometry was conducted. Effects of material yield strength and local fracture toughness were assessed. Different crack lengths were considered to examine relative crack growth rates predicted for different geometries.

IV Debonding Simulations

A series of debonding simulations were undertaken to investigate the two-dimensional Mode I crack growth of HY-100 steel for two different crack-length-to-specimen-width ratios (a_0/w) of 0.136 and 0.250 in a modified compact tension specimen geometry. Additional material responses based on the HY-100 data, but with different yield strengths and ductilities, were also considered. The two dimensional simulations provided quantitative insight into both the physical and computational aspects of stable crack growth in ductile alloys. The modeling techniques also serve as logical prerequisites to full three dimensional modeling in the future. Specific details of the simulations are discussed below.

Specimen Geometries and Loading - Modified compact tension specimen geometries (Figure 1) were selected after a series of preliminary geometry and finite element mesh refinement studies. Applied stress loading at the upper left region of the specimen was used to generate crack opening deformation. This loading produced stable crack growth and was a computationally efficient method of approximating the effect of standard compact tension specimen loading holes. (Models with loading holes in a mesh of this type were found to induce plastic hinge formation in material between the hole and free surface early in the loading history. The resulting load and crack growth were suppressed compared to that observed in laboratory specimens. Plastic hinge formation is not observed for actual laboratory specimens and may be attributed to the two dimension idealization of a three dimensional process and mesh size used in that region of the model.)

Material Responses - Material parameters for the computational simulations (Figure 2) were based on the nonlinear Cauchy stress versus logarithmic strain curve for HY-100 steel. The response of HY-100 steel is representative of extremely ductile steel alloy response. The HY-100 steel nonlinear stress versus strain parameters (Figures 2c, 2d and 2e) used in the analysis were previously obtained with demonstrated accuracy at large strains (Matic, Kirby and Jolles, [26]). The influence of material strength on specimen strength and crack growth was considered by introducing lower (Figure 2a and 2b) and higher yield stress (Figure 2f and 2g) material parameters. The nonlinear form of each high and low yield stress curve, beyond the yield point, followed from the moderate yield HY-100 response. The HY-100 stress versus strain curves exhibited a yield stress of 7.17×10^2 MN/m^2 (1.04×10^5 lb/in^2). The high and low yield stress curves were shifted by plus and minus 1.37×10^2 MN/m^2 (2.00×10^4 lb/in^2), respectfully, to 6.80×10^2 MN/m^2 (0.84×10^5 lb/in^2) and 8.54×10^2 MN/m^2 (1.24×10^5 lb/in^2).

An incremental rate independent plasticity theory was used for the material constitutive model [27]. This standard model for plasticity is summarized here for completeness. Total strains in the multiaxial strain state ε_{ij} were obtained by the integration of the linearly decomposed rate of deformation tensor D_{ij}. This integration was performed under the assumption

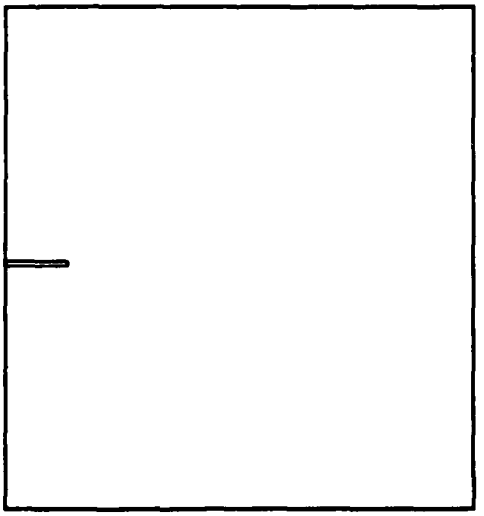

(a)

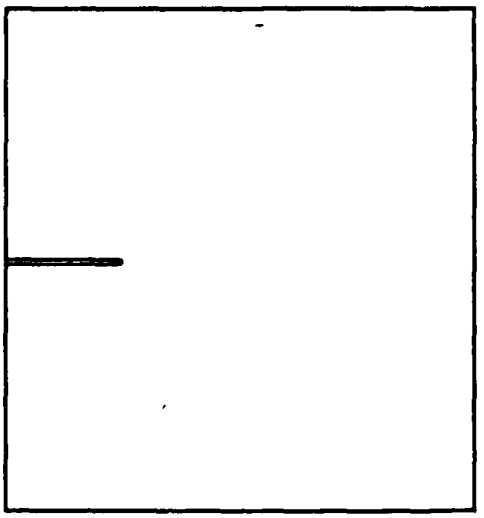

(b)

Fig. 1 — Ductile simulation geometries (a) short crack length, $a_0/w=0.136$, (b) long crack length, $a_0/w=0.25$.

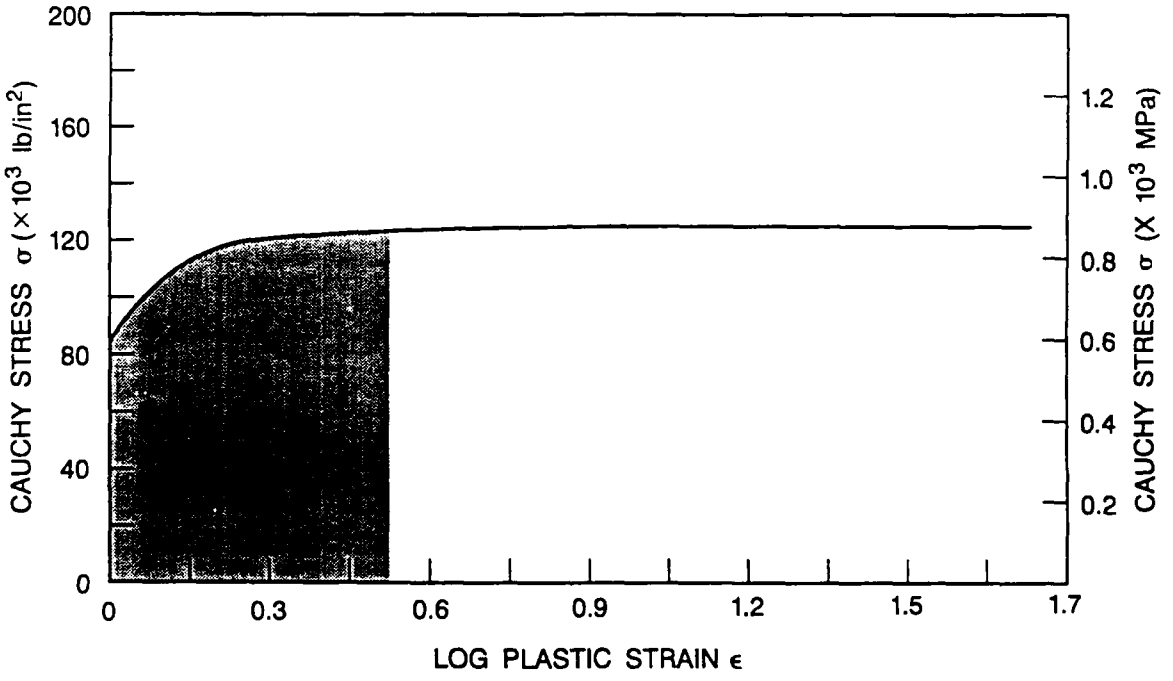

(a)

Fig. 2 — Cauchy stress versus log strain curves for yield stress (× 10^2 MN/m^2) — fracture toughness (× 10^2 MN-m/m^3) combinations (a) 5.79-4.41, (b) 5.79-13.23, (c) 7.17-4.41, (d) 7.17-8.83, (e) 7.17-13.23, (f) 8.55-4.41, (g) 8.55-13.23

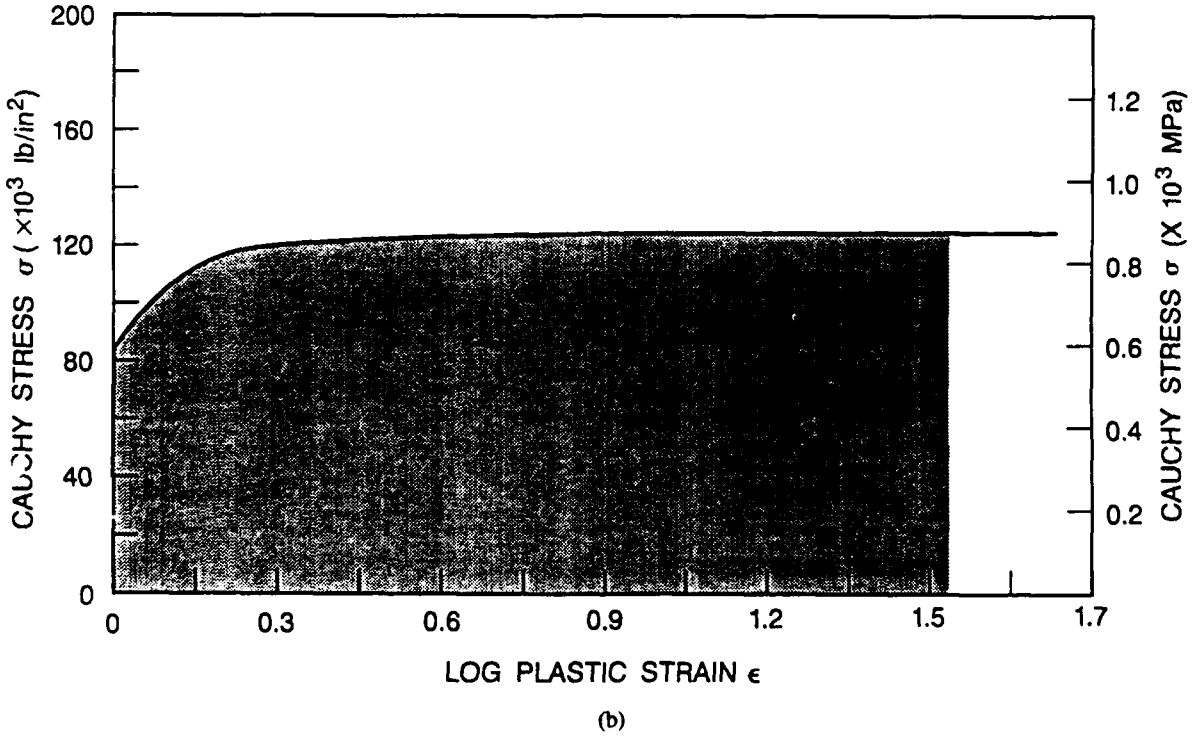

(b)

Fig. 2 (Continued) — Cauchy stress versus log strain curves for yield stress (× 10^2 MN/m^2) — fracture toughness (× 10^2 MN-m/m^3) combinations (a) 5.79-4.41, (b) 5.79-13.23, (c) 7.17-4.41, (d) 7.17-8.83, (e) 7.17-13.23, (f) 8.55-4.41, (g) 8.55-13.23

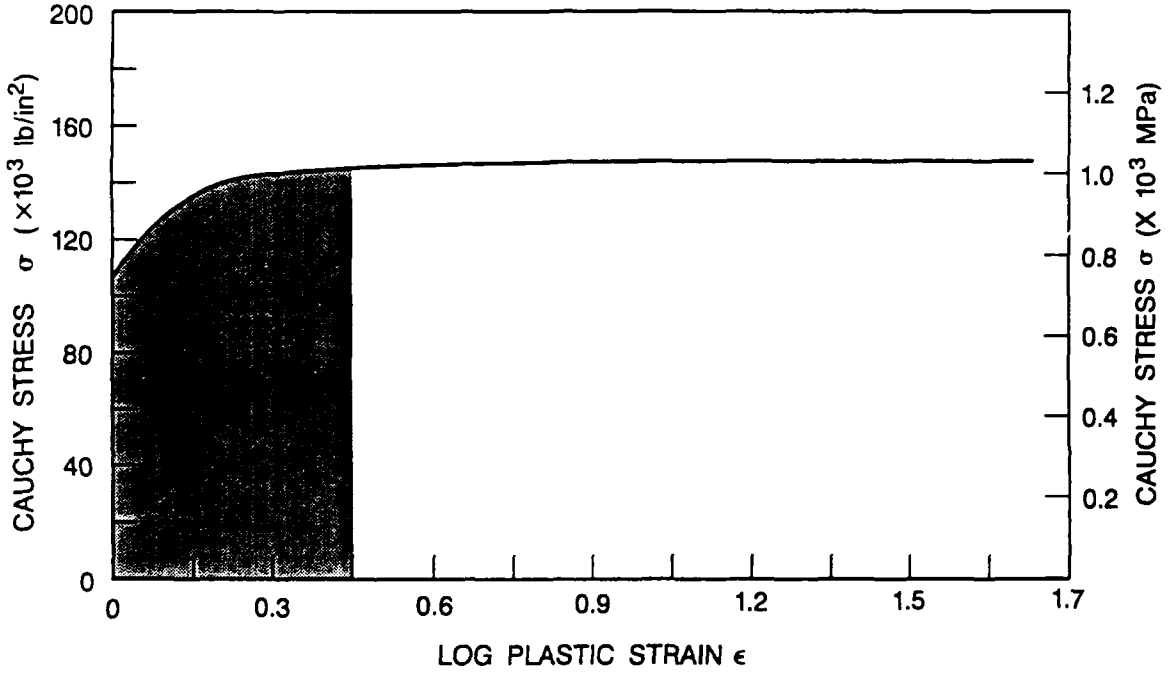

(c)

Fig. 2 (Continued) — Cauchy stress versus log strain curves for yield stress (× 10^2 MN/m^2) — fracture toughness (× 10^2 $MN\text{-}m/m^3$) combinations (a) 5.79-4.41, (b) 5.79-13.23, (c) 7.17-4.41, (d) 7.17-8.83, (e) 7.17-13.23, (f) 8.55-4.41, (g) 8.55-13.23

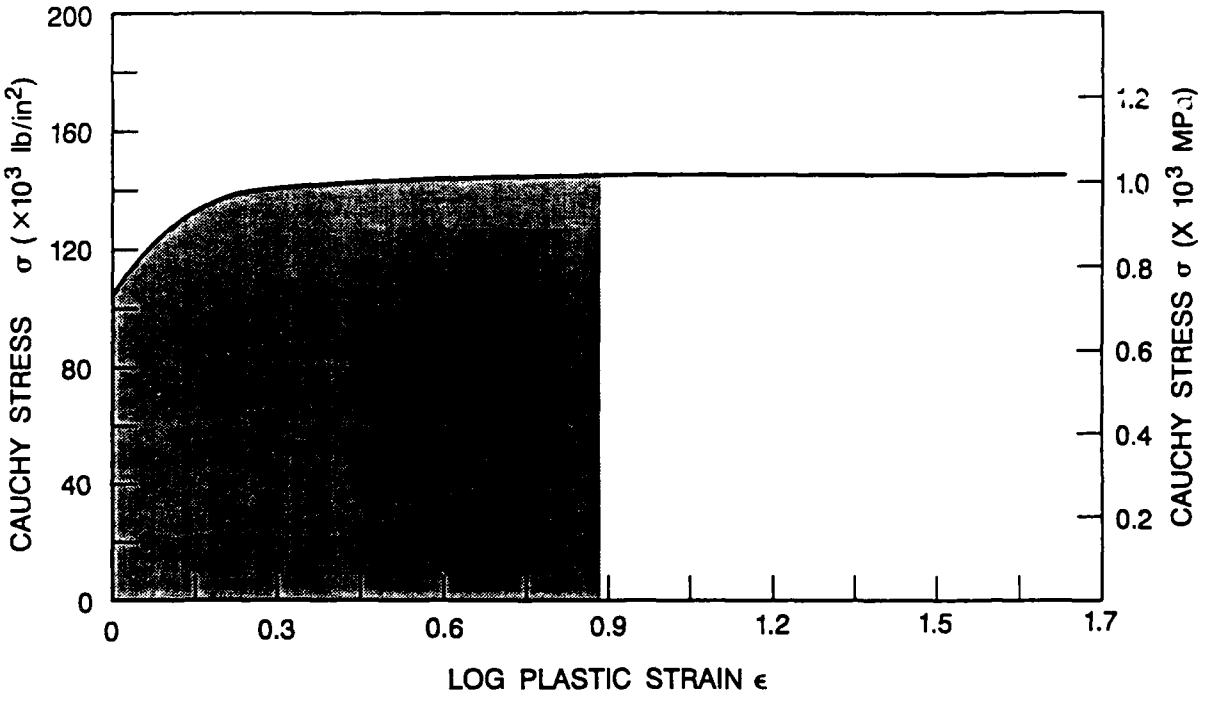

(d)

Fig. 2 (Continued) — Cauchy stress versus log strain curves for yield stress (× 10^2 MN/m^2) — fracture toughness (× 10^2 MN-m/m^3) combinations (a) 5.79-4.41, (b) 5.79-13.23, (c) 7.17-4.41, (d) 7.17-8.83, (e) 7.17-13.23, (f) 8.55-4.41, (g) 8.55-13.23

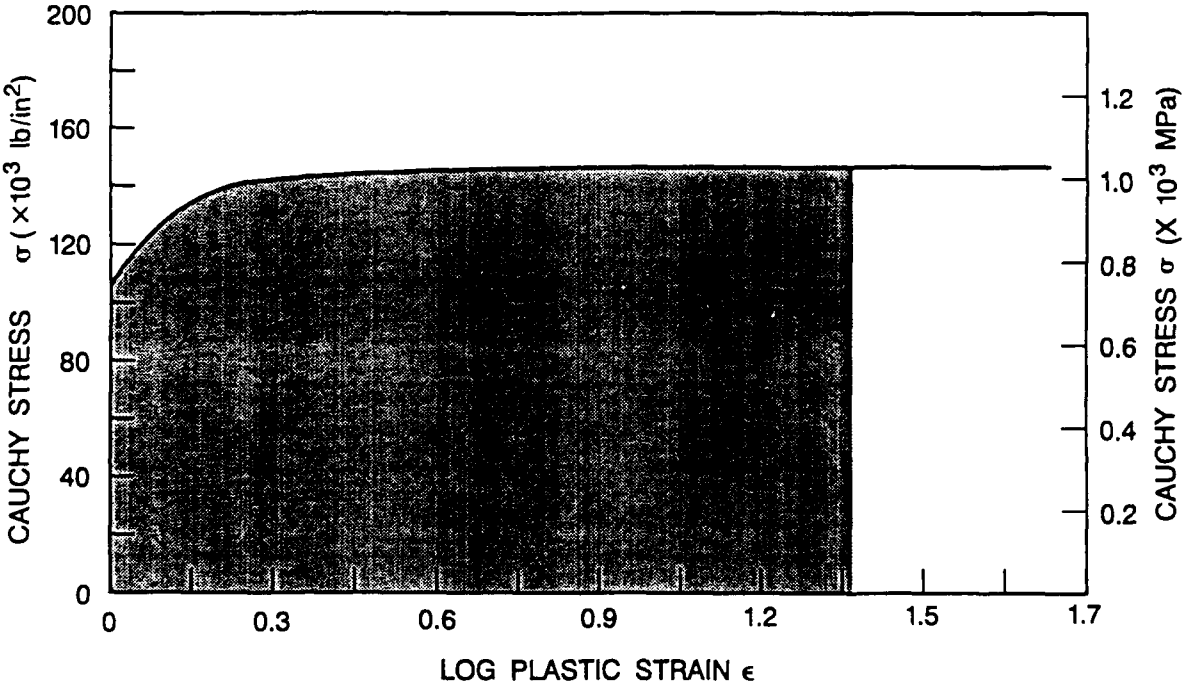

(e)

Fig. 2 (Continued) — Cauchy stress versus log strain curves for yield stress (× 10^2 MN/m^2) — fracture toughness (× 10^2 MN-m/m^3) combinations (a) 5.79-4.41, (b) 5.79-13.23, (c) 7.17-4.41, (d) 7.17-8.83, (e) 7.17-13.23, (f) 8.55-4.41, (g) 8.55-13.23

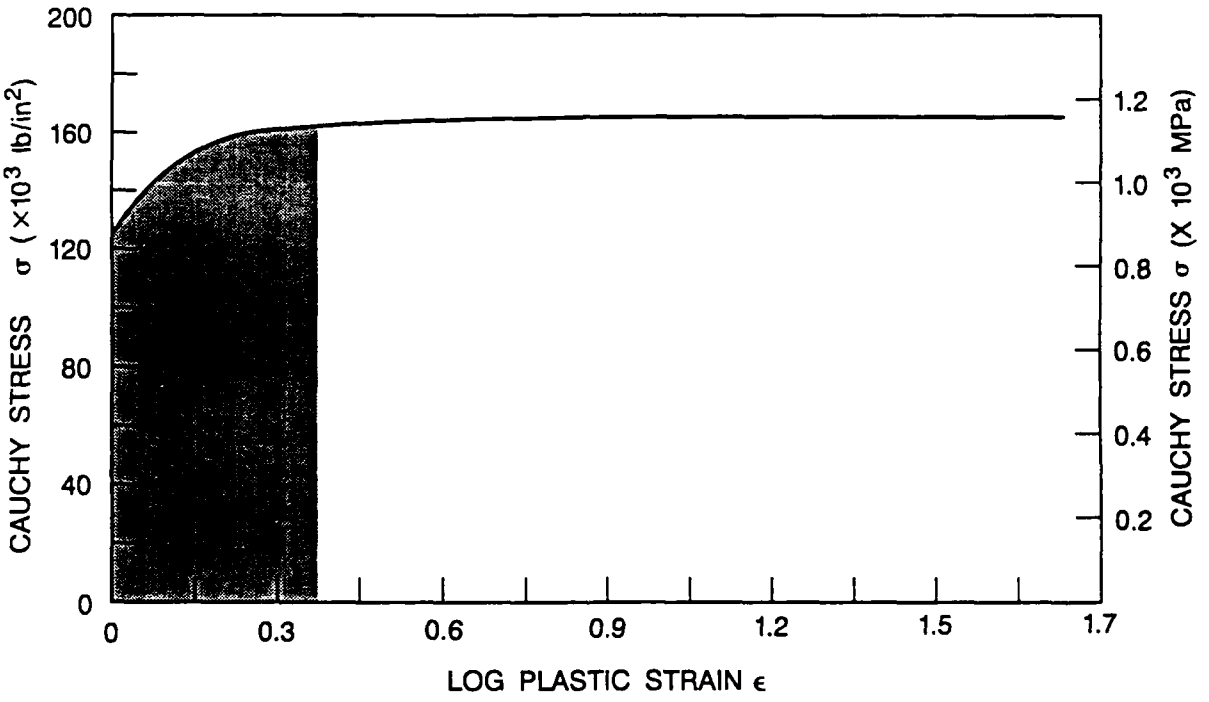

(f)

Fig. 2 (Continued) — Cauchy stress versus log strain curves for yield stress ($\times 10^2$ MN/m^2) — fracture toughness ($\times 10^2$ MN-m/m^3) combinations (a) 5.79-4.41, (b) 5.79-13.23, (c) 7.17-4.41, (d) 7.17-8.83, (e) 7.17-13.23, (f) 8.55-4.41, (g) 8.55-13.23

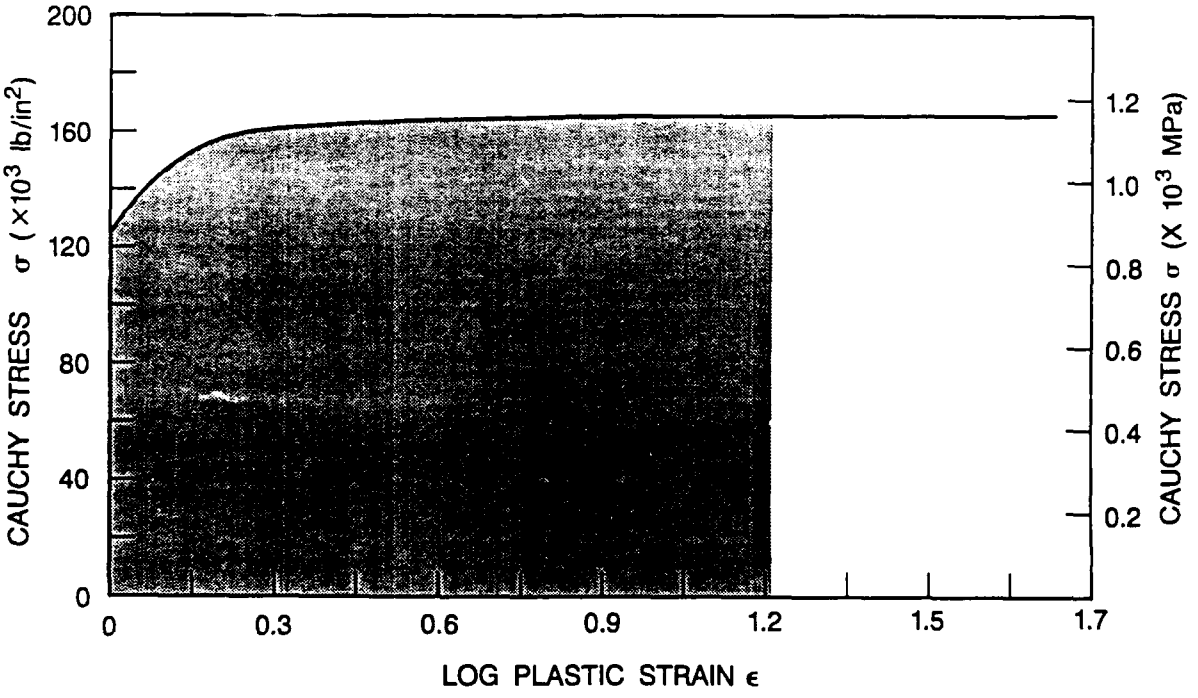

(g)

Fig. 2 (Continued) — Cauchy stress versus log strain curves for yield stress ($\times 10^2$ MN/m^2) — fracture toughness ($\times 10^2$ MN-m/m^3) combinations (a) 5.79-4.41, (b) 5.79-13.23, (c) 7.17-4.41, (d) 7.17-8.83, (e) 7.17-13.23, (f) 8.55-4.41, (g) 8.55-13.23

that the elastic strains remain infinitesimal, as are the cases in this investigation. The total multiaxial strain state ε_{ij}, expressed in terms of elastic and plastic components, was

$$\varepsilon_{ij} = \varepsilon^e_{ij} + \varepsilon^p_{ij} \tag{1}$$

The total logarithmic uniaxial strain ε, consistent with the integration of the rate of deformation tensor for a multiaxial strain state, was decomposed as

$$\varepsilon = \varepsilon^e + \varepsilon^p \tag{2}$$

The yield function f takes the form

$$f(\tau_{ij}) = \tau(\varepsilon^p) \tag{3}$$

where τ_{ij} and τ are the multiaxial Kirchoff (or Treffetz) and uniaxial stress states, respectively. The associated flow rule governed plastic strain increments by the relation

$$d\varepsilon^p_{ij} = \lambda \frac{\partial f}{\partial \tau_{ij}} \tag{4}$$

In the case of purely elastic behavior $\lambda = 0$. For active material yielding

$$\lambda > 0 \tag{5}$$

$$\lambda = d\varepsilon^p \frac{\tau}{\tau_{ij} \dfrac{\partial f}{\partial \tau_{ij}}} \tag{6}$$

Plastic strain increments also satisfied a dissipation equivalence condition

$$\tau \, d\varepsilon^p = \tau_{ij} \, d\varepsilon^p_{ij} \tag{7}$$

and a consistency condition

$$\frac{\partial f}{\partial \tau_{ij}} d\tau_{ij} - \frac{\partial \tau}{\partial \varepsilon^p} d\varepsilon^p = 0 \qquad (8)$$

The von Mises yield function

$$f(\tau_{ij}) = \frac{3}{2} (s_{ij} s_{ij})^{\frac{1}{2}} \qquad (9)$$

was employed. The deviatoric stress tensor s_{ij} was defined as

$$s_{ij} = \tau_{ij} - \frac{1}{3} \tau_{kk} \delta_{ij} \qquad (10)$$

where the hydrostatic component of stress is $\tau_{kk}/3$.

The Kirchoff stress and logarithmic strain measures are employed because of advantages gained in computational implementation. The Kirchoff stress tensor τ_{ij} is approximately equal to the more physically motivated Cauchy stress tensor σ_{ij} for deformations involving only small changes in volume. This condition was implicit in these analyses. The uniaxial Cauchy stress - log strain constitutive response of the material was formally input, in multilinear form, as Cauchy stress and logarithmic strain pairs for the ABAQUS program.

Local Fracture Toughness Criterion - The material fracture toughness, as characterized by the absorbed strain energy density at fracture, has been determined to vary by at least fifty percent in the case of HY-100 steel [26] subjected to different local stress versus strain histories. The role of multiaxial loading histories affects both inelastic deformation and fracture. Fractographic dependence for HY-100 steel has been examined by Harvey and Jolles [28] who found significant differences in relative microvoid and cleavage proportions on cylinderical tensile specimen fracture surfaces. Correlation between these microstructural differences and the absorbed strain energy density at the point of initial material fracture was also demonstrated.

In order to examine the influence of a local fracture toughness value on crack growth, the path dependent aspects of fracture toughness were suppressed by considering a constant critical absorbed strain energy density for each computational simulation, i.e.

$$w_c = \text{constant}. \qquad (11)$$

The actual path dependent of the toughness was used to select the range of w_c values for the simulations. Three different critical energy density values were used. The low, moderate and high local fracture toughness values were 4.41, 8.83 and 13.23 x 10^2 MN-m/m^3 (64.0, 128.0 and 192.0 x 10^3 lb-in/in^3). The moderate and high values were based on the range of path dependent critical HY-100 values obtained from the solution procedure discussed previously [26]. The importance of this range to material fracture and crack initiation of HY-100 steel compact tension specimens has also been previously demonstrated DeGiorgi, Kirby and Jolles [18]. The low value was selected to simulate what could be expected if composition or structure changes were induced in the material by processes such as welding.

Computational Model - The ABAQUS finite element code Version 4.8 was used for the computational simulations [29]. Finite element models for the simulations are shown in Figure 3. Specimen symmetry required that only one half of the specimen be modeled. The initial crack faces and crack propagation path lie on the symmetry axis.

Type CPE8 and CPE8H plane strain elements were used to model the solid. Both element types are 8-noded quadrilateral elements with quadratic displacement interpolation. The CPE8H elements also include an independently interpolated linear hydrostatic stress. The CPE8H elements were employed in elements near crack tip to sustain the anticipated large strain, essentially constant volume deformation. Interface elements, type INTER3, bonded the material elements adjacent to the Mode I crack propagation path to the line of symmetry. The interface elements were the means by which nodal force release was implemented.

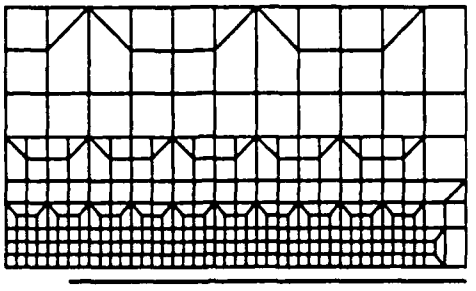

(a)

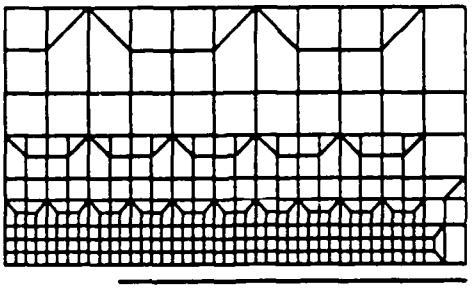

(b)

Fig. 3 - Finite element models for ductile tear simulations (a) short crack length, (b) long crack length

All analyses were performed with full geometric nonlinearity to account for large strains and large rotations. An updated Lagrangian formulation was used for incremental solution in ABAQUS. A modified Rik's algorithm, being load and displacement controlled, was used to enhance numerical stability.

Stress boundary conditions were applied at the upper left portion of the model to approximate the stress applied at a loading hole in an actual compact fracture specimen. More detailed consideration of the loading hole, as considered in [18], would have increased the model size but not provided any additional substantive information on crack growth, crack length effects or material effects.

Debonding Algorithm - An automated approach to quasistatic crack propagation was implemented in the ABAQUS Version 4.8 finite element program. The approach was based on the debonding of finite elements, through the local fracture criterion and nodal force release, to create new fracture surface during the load application. Nodal release was implemented through the use of the interface elements which enforced displacement continuity across a specified crack propagation path ahead of the crack tip. The crack path was specified in the model by a list of nodes ahead of the crack tip. Interface elements associated with the crack path were also specified.

A subroutine, written by the user and executed by the ABAQUS program, was used to determine the value of a debond parameter c at each node of the crack path ahead of the current crack tip. The parameter c, defined as the difference between the absorbed strain energy density w and associated critical value of the critical strain energy density w_c, were associated with each node in the crack path through the user subroutine. That is,

$$c = w - w_c$$

The value of c was used to control the debonding sequence used to predict crack propagation along the specified path (Figure 4). Fracture occured when the debond parameter at the crack tip passed from negative to positive values, reflecting an excess of absorbed strain energy density over

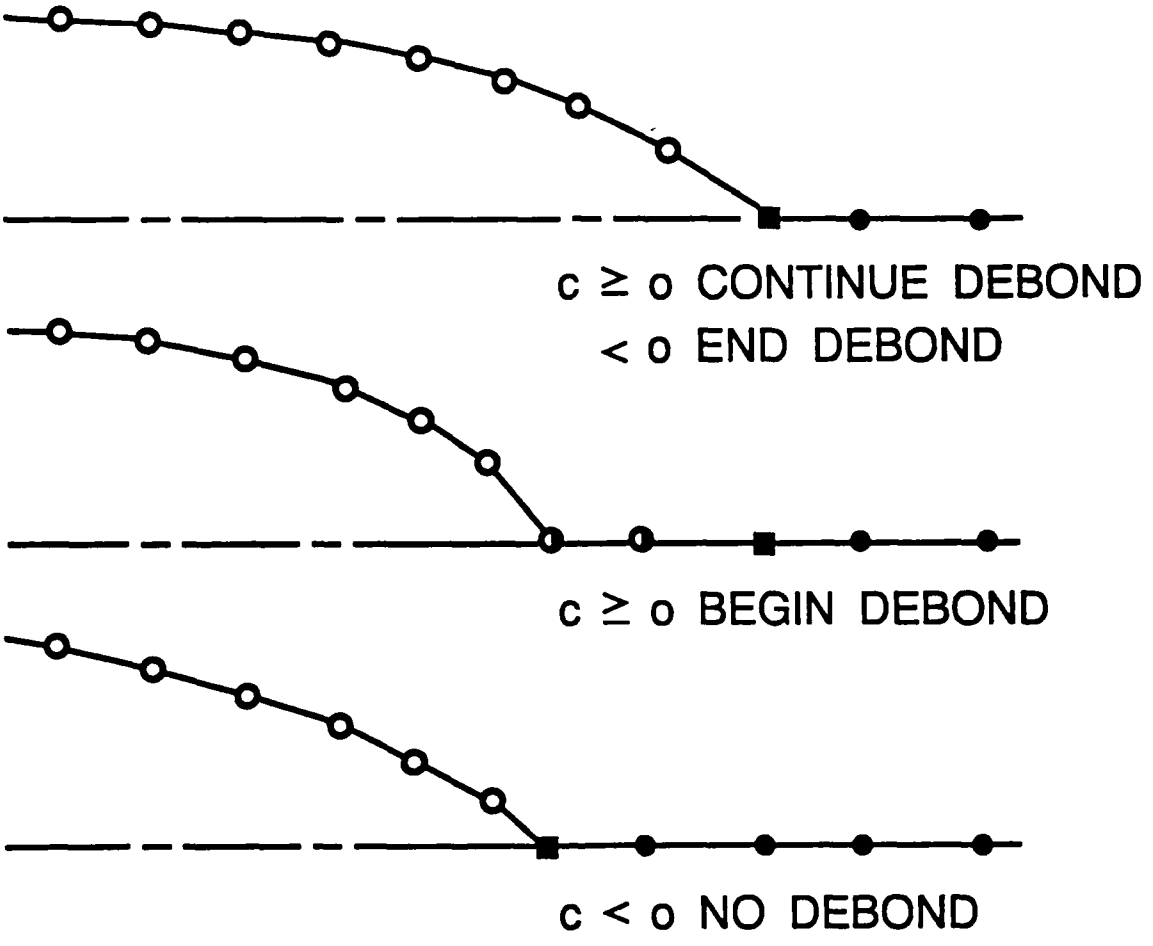

Fig. 4 — Schematic of debonding algorithm

the material's capacity to sustain such an energy density. In general, a load increment did not produce a value of c equal to zero. Rather, c would exceed zero for the solution increment when crack growth should occur. The debonding algorithm interpolated over the normal load increment to generate an intermediate load increment leading up to debonding which more closely approximated a c value of zero.

Crack propagation occured in discrete increments, one element at a time. The energy density parameters were calculated during each load increment from the material constitutive model and the local material fracture toughness criterion. Required information was obtained from the finite element database by the user subroutine.

When the debonding sequence for an element was activated the load was increased by a small fraction of the current load. Therefore, crack propagation occured under essentially constant load. The two nodes of the eight noded finite elements in the crack path immediately ahead of the current crack tip, i.e. one corner and one midside node, were released by removing displacement constraints and reaction forces. The displacement constraints were removed immediately. Nodal forces were removed in equal increments. Five equal increments were used in this investigation. Equilibrium was reestablished by the program for the new crack length. The fracture criterion was examined to see if crack growth should continue at the current load. If the fracture criterion was satisfied, crack growth continues at the same step in the load history. If the criterion was not satisfied, loading proceeds to the next increment. Stable crack growth was viewed as a process of continuous loading accompanied by intermittent debonding. Unstable crack growth, if it occurred, would be viewed as continuous debonding in the absence of additional active loading.

The simulations conducted for both long and short crack length geometries are summarized in Table 2. The extreme values of all strength and local fracture toughness combinations were examined, as were all local fracture toughness values for the HY-100 constitutive response. These simulations were identified by an abbreviation of the form GMMFFF and associated symbols in the graphical results. G denotes the short (S) or long (L)

Yield Stress,		Local Fracture Toughness, x 10^2 MN-m/m^3		
x 10^2 MN/m^2		Low	Moderate	High
		4.41	8.83	13.23
High	8.55	X	-	X
Moderate	7.17	X	X	X
Low	5.79	X	-	X

Table 2 Material Parameter Variations Analyzed for Short and Long Crack Length Geometries

crack geometry and is represented by open and closed symbols, respectively, on all graphs. MM is the material yield strength. Low (-2), moderate (HY), and high (+2) yield stresses are represented by circles, triangles and squares. FFF is the local fracture toughness. Low (064), moderate (128) or high (192) critical absorbed energy density parameters are indicated by dotted, dashed and solid lines, respectively.

The debond criterion was explicitly based on nodal averaged values of energy density calculated from adjacent element nodal averages. As is common in high gradient regions of a finite element analysis, the nodal averaged value may not be an accurate indication of material response immediately ahead of the crack. Specifically, the nodal average will be greater than the value behind the crack and less than the value ahead of the crack. To achieve a more consistent interpretation of the nodal averaged value for debonding, a proportionality factor was used to relate the nodal averaged energy density values to the energy density values of the material in the element ahead of the crack tip. This factor, based on data in previous studies [18], reduced the low, moderate and high critical energy density values to 2.41, 4.83 and 7.23 x 10^2 MN-m/m^3 (35.0, 70.0 and 105.0 x 10^3 lb-in/in^3), respectively, for purposes of numerical implementation in the debonding algorithm. The physical response of the material and the fracture toughness value are therefore both considered by the proportionality factor in a consistent manner.

V Results

The results of the crack growth simulations are presented here in terms of local material responses and global specimen responses.

The strain energy density ratio (w/w_c) at the current crack tip is plotted against crack mouth opening displacement (CMOD). For the three materials involving the moderate yield strength parameters associated with HY-100 steel the short crack length results are shown in Figure 5 and the long crack length results are shown in Figure 6. The four extreme yield strength and local fracture toughness parameter combinations for the short crack length and the long crack length are shown in Figure 7 and Figure 8.

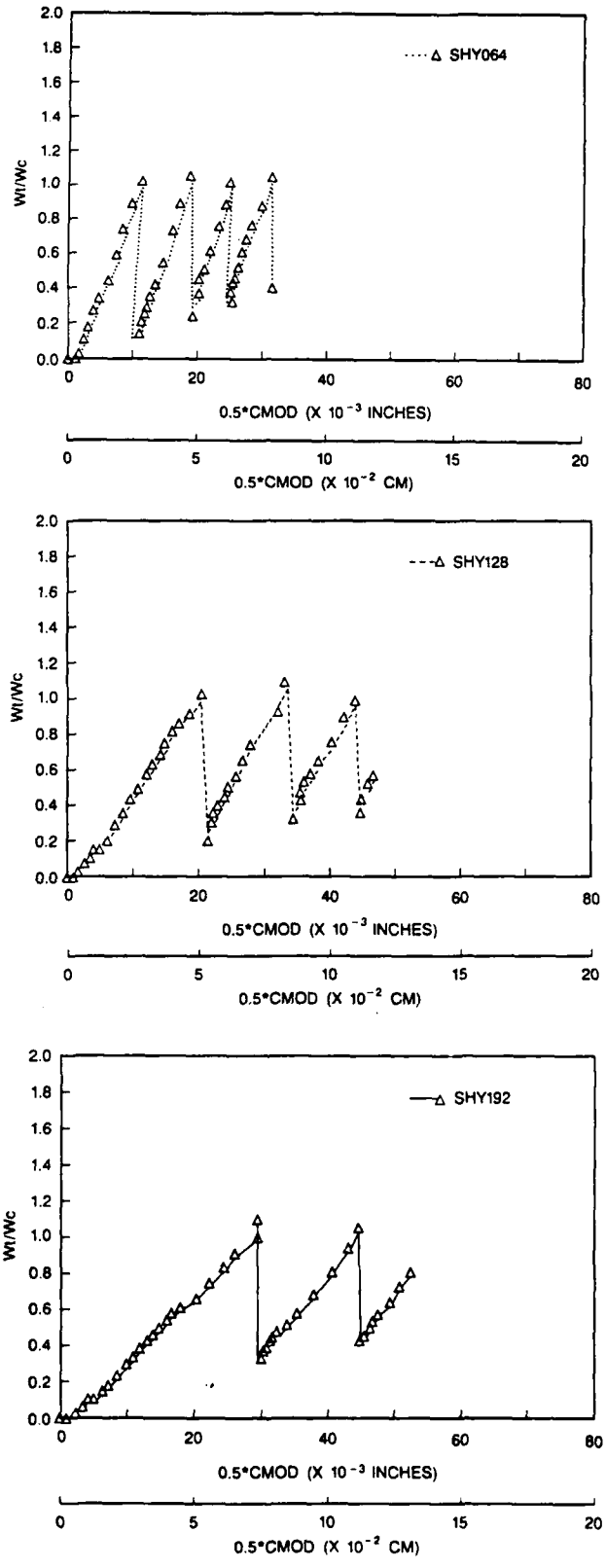

Fig. 5 Strain energy density ratio (w/w_c) at the crack tip versus crack mouth opening displacement (CMOD) for HY-100 short crack length, 7.17 × 10^2 MN/m^2 ksi yield stress, and (a) 4.41, (b) 8.83 and (c) 13.23 × 10^2 MN-m/m^3 local fracture toughness values

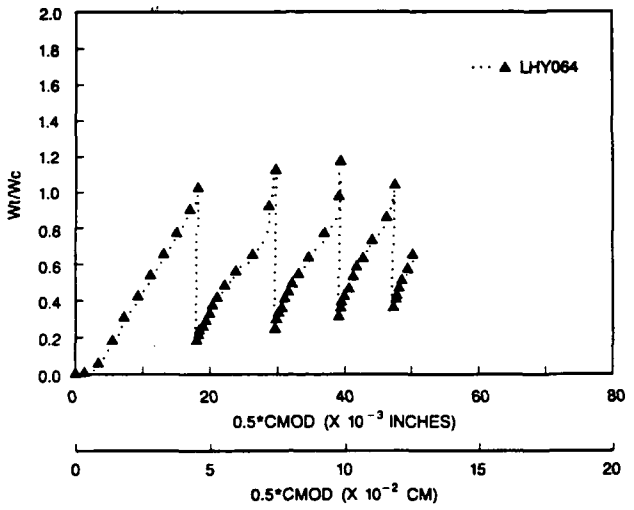

(a)

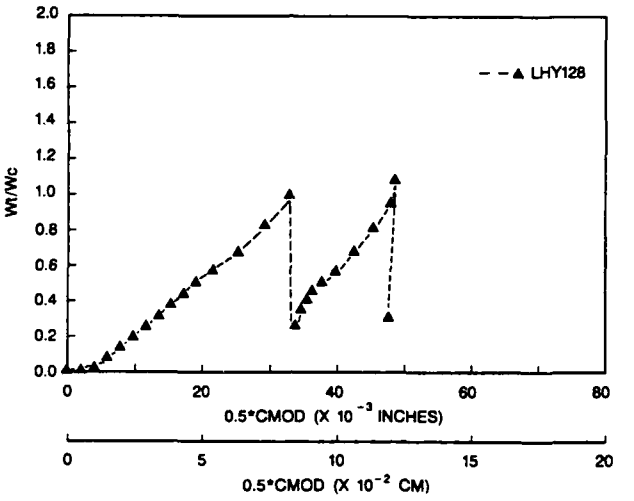

(b)

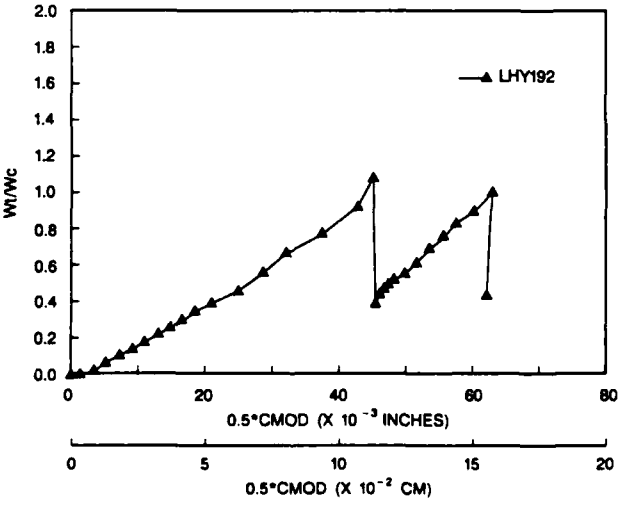

(c)

Fig. 6 — Strain energy density ratio (w/w_c) at the crack tip versus crack mouth opening displacement (CMOD) for HY-100 long crack length, 7.17 × 10^2 MN/m^2 yield stress, and (a) 4.41, (b) 8.83 and (c) 13.23 × 10^2 MN-m/m^3 local fracture toughness values

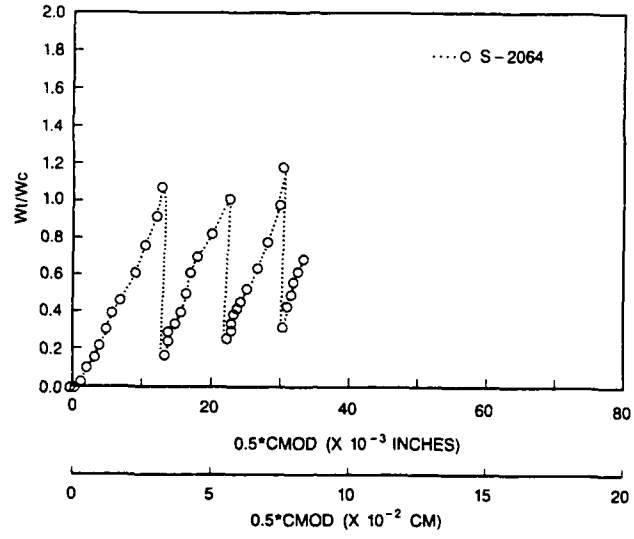

(a)

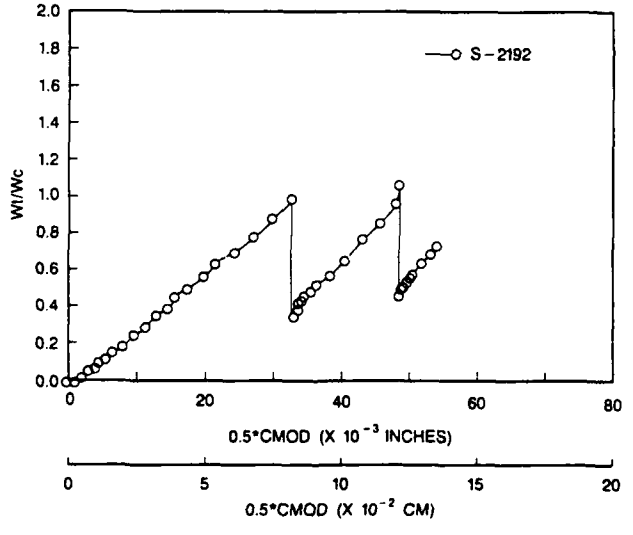

(b)

Fig. 7 — Strain energy density ratio (w/w_c) at the crack tip versus crack mouth opening displacement (CMOD) for short crack length geometry and extreme combinations of strength and toughness. Yield stress of 5.79×10^2 MN/m^2 and (a) 4.41 and (b) 13.23×10^2 MN-m/m^3 local fracture toughness values. Yield stress of 8.55×10^2 MN/m^2 and (c) 4.41 and (d) 13.23×10^2 MN-m/m^3 local fracture toughness values.

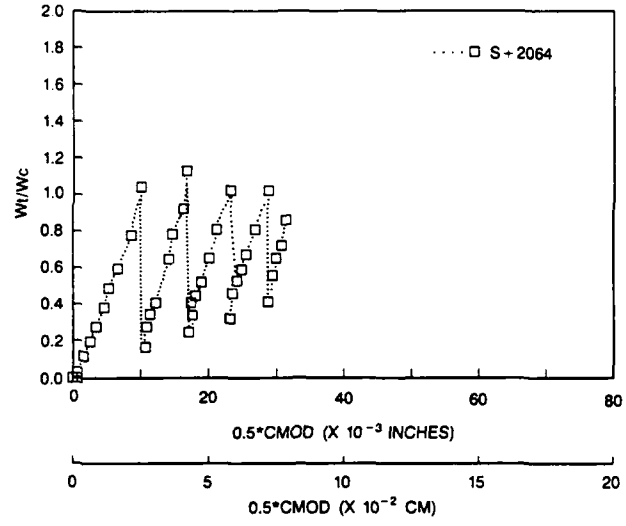

(c)

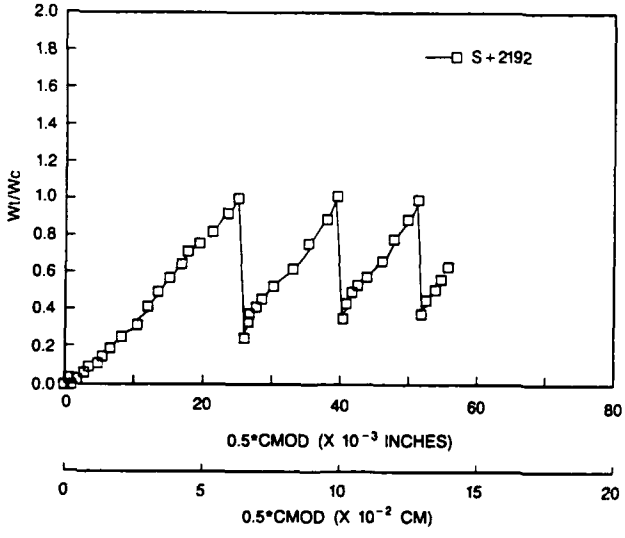

(d)

Fig. 7 (Continued) — Strain energy density ratio (w/w_c) at the crack tip versus crack mouth opening displacement (CMOD) for short crack length geometry and extreme combinations of strength and toughness. Yield stress of 5.79×10^2 MN/m^2 and (a) 4.41 and (b) 13.23×10^2 MN-m/m^3 local fracture toughness values. Yield stress of 8.55×10^2 MN/m^2 and (c) 4.41 and (d) 13.23×10^2 MN-m/m^3 local fracture toughness values.

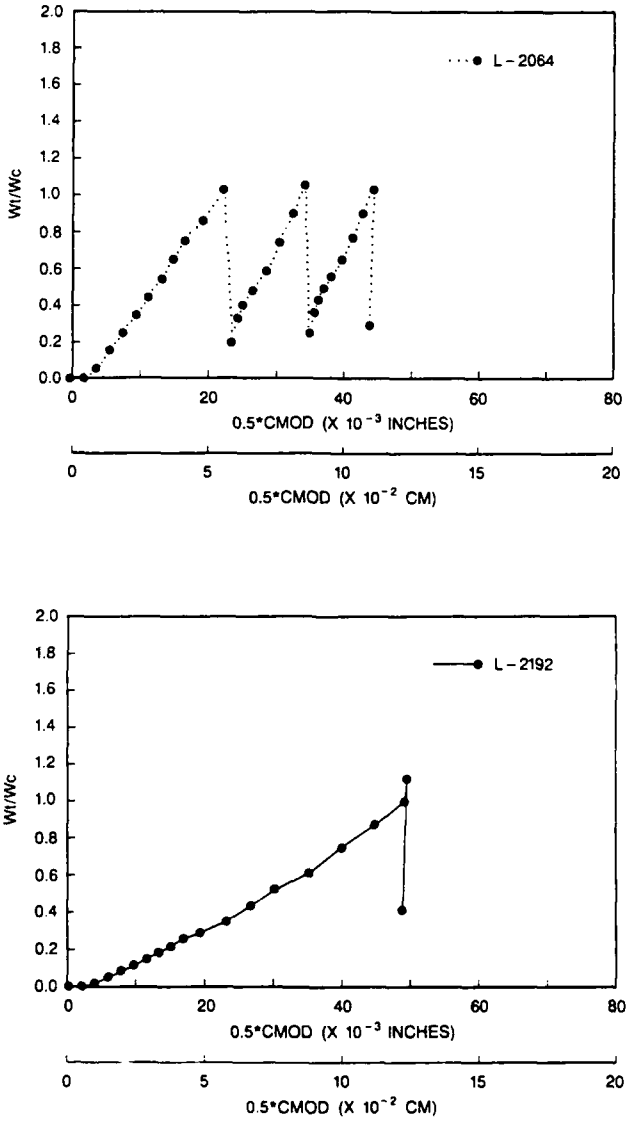

Fig. 8 — Strain energy density ratio (w/w_c) at the crack tip versus crack mouth opening displacement (CMOD) for long crack length geometry and extreme combinations of strength and toughness. Yield stress of 5.79×10^2 MN/m^2 and (a) 4.41 and (b) 13.23×10^2 MN-m/m^3 local fracture toughness values. Yield stress of 8.55×10^2 MN/m^2 and (c) 4.41 and (d) 13.23×10^2 MN-m/m^3 local fracture toughness values.

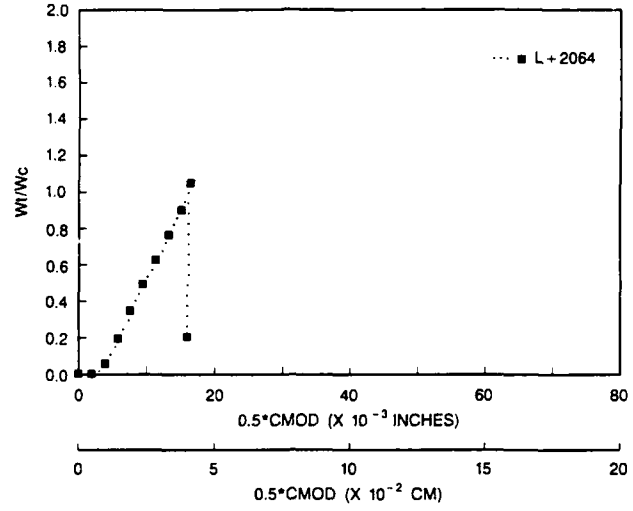

(c)

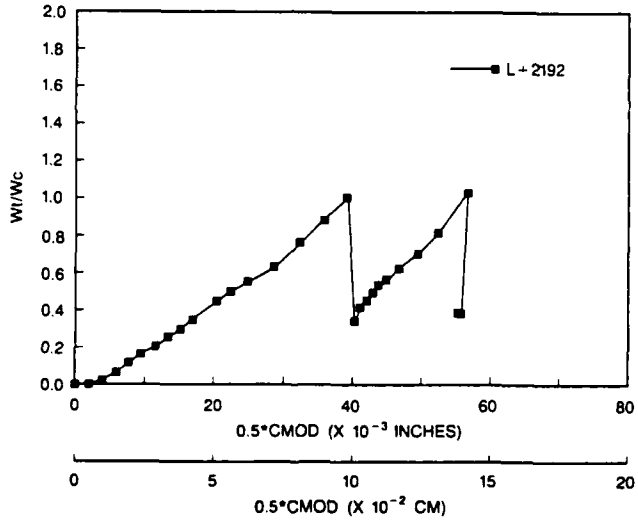

(d)

Fig. 8 — (Continued) Strain energy density ratio (w/w_c) at the crack tip versus crack mouth opening displacement (CMOD) for long crack length geometry and extreme combinations of strength and toughness. Yield stress of 5.79×10^2 MN/m^2 and (a) 4.41 and (b) 13.23×10^2 MN-m/m^3 local fracture toughness values. Yield stress of 8.55×10^2 MN/m^2 and (c) 4.41 and (d) 13.23×10^2 MN-m/m^3 local fracture toughness values.

The strain energy density ratio normalizes the material damage with respect to the material resistance to fracture at any point in the specimen over the loading history. The rate at which a point in the specimen approaches fracture is reflected in the slope of the curve. A strain energy density ratio of one corresponds to material fracture and initiation of the debonding process.

The current crack tip position is redefined by the debonding process when crack growth takes place. The energy density ratio of the material at the new crack tip again represents the local resistance to fracture .The new crack tip must pass through this material if crack growth is to be sustained. For the computational simulations of this study, the decrease in strain energy density ratio observed after each successive crack growth increment of one element results in a new stable crack length. For each successive crack growth increment, however, the energy density ratio of the material at the new crack tip is greater than the energy density ratio at the time the prior crack tip was defined by debonding. This trend, as defined by the energy density ratios at successive crack tip definitions, is an indication of the rate at which stable crack growth leads to crack instability. For those material parameters considered for which multiple debonding increments occurred, it is apparent that more than ten total crack growth increments would be required, at the present rate of post-increment energy ratio increase, to produce repetitive debonding and crack instability. More than ten increments of crack growth would place the crack tip well into the center portion of the specimen width. The range of parameter values would generally suggest this for all cases considered.

Physically, HY-100 steel in compact fracture specimen geometries is observed to sustain extensive stable crack growth at the leading edge of the crack, in the center of the specimen, extending over more than one half the specimen width. The crack growth at the free surface lags far behind, resulting in the classical curved crack front which tunnels into the specimen. (Plastic hinge formation occurs as the crack approaches the free surface of the specimen ahead of the crack. Final specimen failure follows.) The physical response is an inherently three dimensional process, while the simulations were two dimensional. The nature of these results are, however, consistent

with the general trends of HY-100 crack growth preceding the gross geometric deformations of plastic hinge formation.

The applied force is plotted against crack mouth opening displacement (CMOD), taken at the corner defined by the intersection of the crack face and free surface behind the crack on the specimen. For the simulations involving HY-100 yield strength the short crack length results are shown in Figure 9 and the long crack length results are shown in Figure 10. The four extreme yield strength and local fracture toughness combinations for the short crack length and the long crack length are shown in Figure 11 and Figure 12. The overall nonlinearity of the response is sustained though increasing values of CMOD. The intermittent unloading on the curves, interrupting the otherwise smooth character of the response, are generated as debonding extends the crack. The unloading occurs during the debond as equilibrium is reestablished by the modified Rik's algorithm for a longer crack and corresponding elastic-plastic crack tip fields. Active loading of the specimen resumes after equilibrium is obtained. Relatively small unloading magnitudes encountered during stable debonding suggests that the discrete debonding is approximating continuous stable crack growth in a satisfactory manner.

It may be noted that the influence of greater material yield stress is directly translated into higher specimen strength. At the same time, crack growth rates are seen to accelerate as the yield stress increases for constant material fracture toughness and specimen geometry. The elastic portion of the material response, locally, and its interaction with the aggregate recoverable response of the specimen, globally, combine to produce conditions favorable to energy dissipation at the crack tip. This apparently accelerates the local fracture process and, therefore, crack growth.

It may also be noted that the influence of material fracture toughness on specimen strength, as seen for the case of HY-100 material yield strength, was most significant when comparing the low to moderate fracture toughness simulations. The relative ability of the specimen to sustain load is increased only slightly when the material fracture toughness was increased from the moderate to high value. A comparison of the uniaxial stress and strain ranges associated with the local fracture toughness values (i.e. Figure 2c) shows that

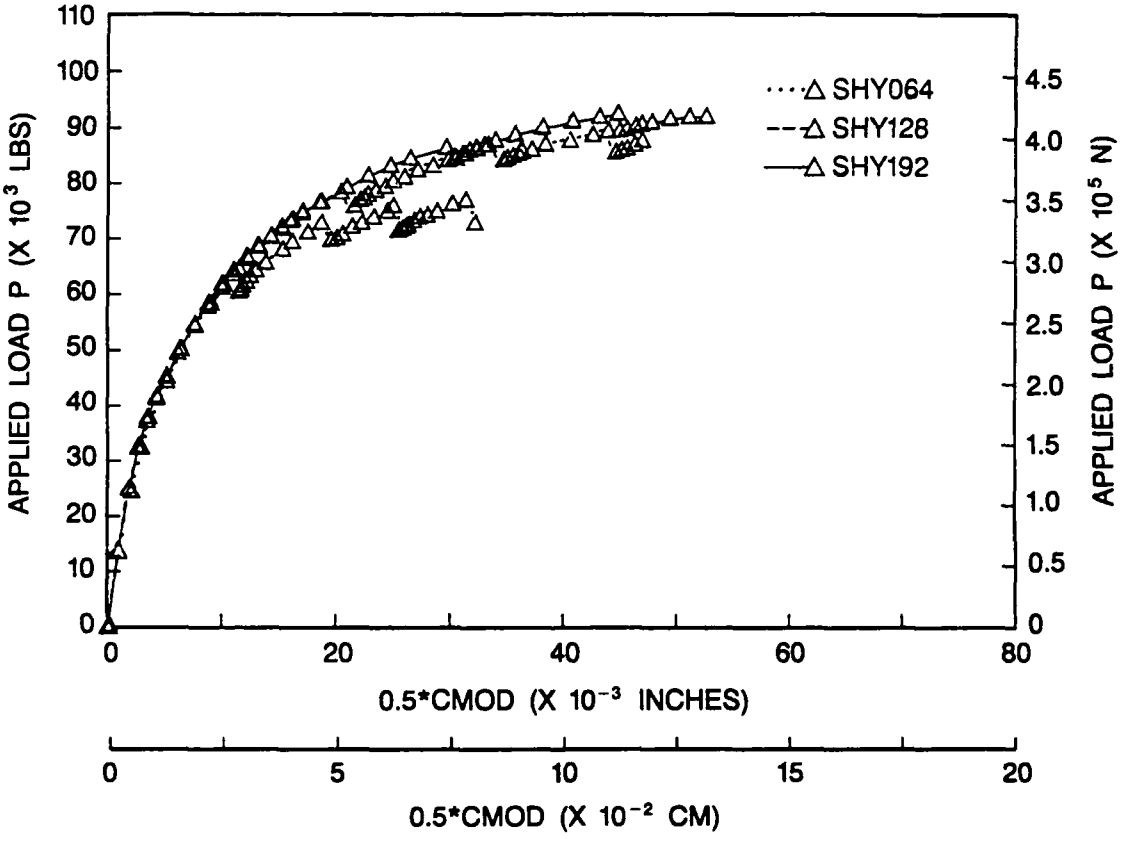

Fig. 9 — Applied load (P) versus crack mouth opening displacement (CMOD) for HY-100. Short crack length, 7.17×10^2 MN/m^2 yield stress and 4.41, 8.83 and 13.23×10^2 MN-m/m^3 local fracture toughness values

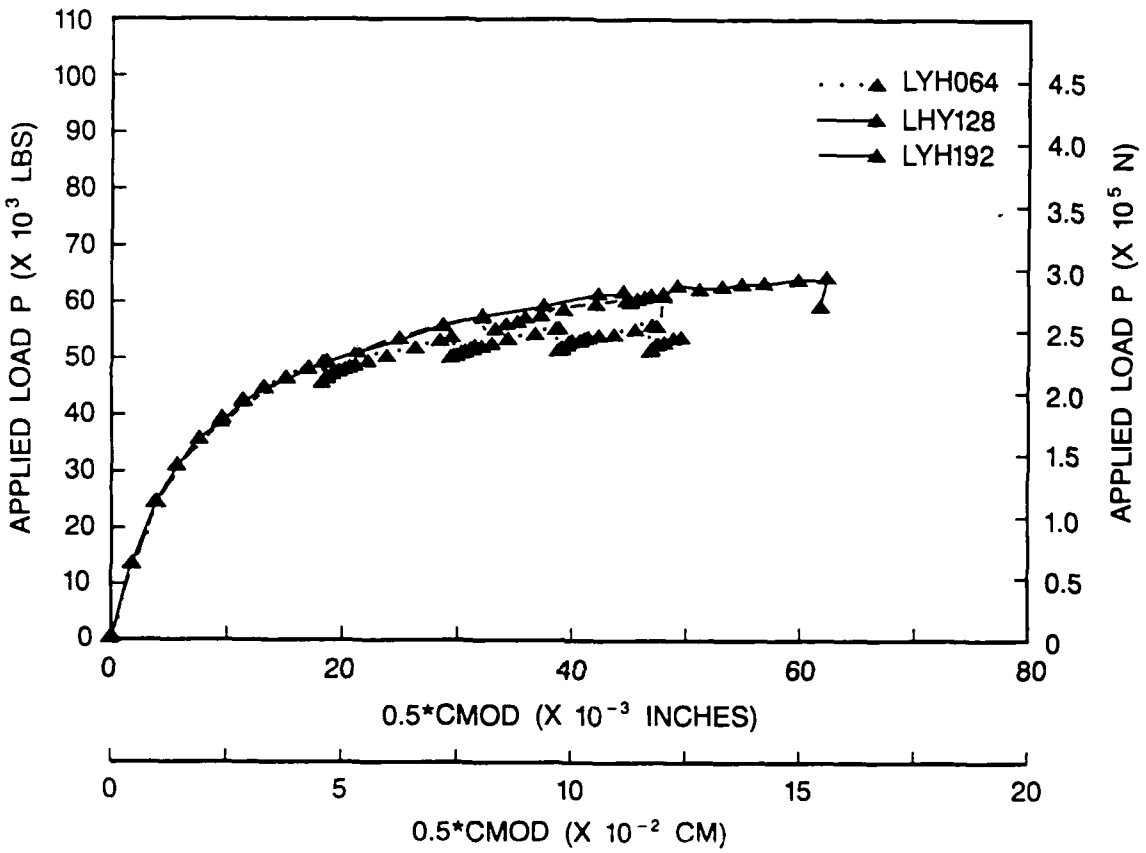

Fig. 10 — Applied load (P) versus crack mouth opening displacement (CMOD) for HY-100. Long crack length, 7.17 × 10^2 MN/m^2 yield stress and 4.41, 8.83 and 13.23 × 10^2 MN-m/m^3 local fracture toughness values.

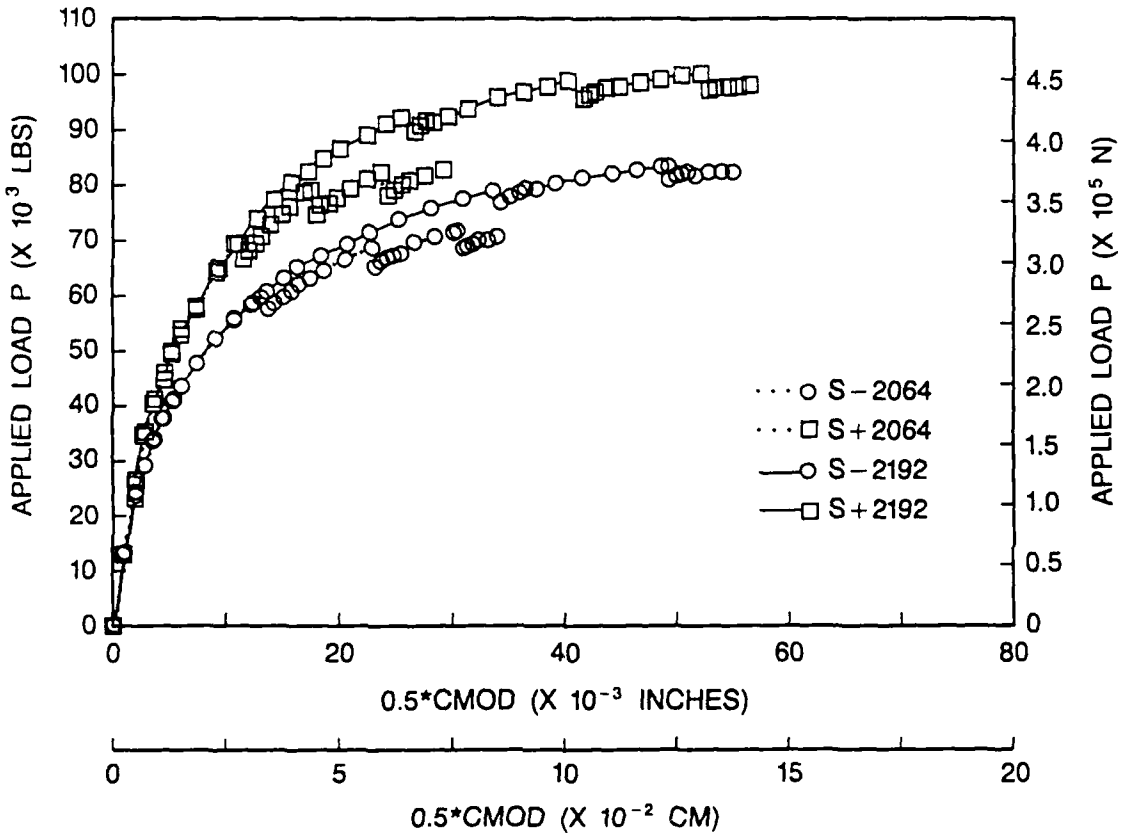

Fig. 11 — Applied load (P) versus crack mouth opening displacement (CMOD) for extreme combinations of strength and toughness. Short crack length, 5.79 and 8.55 × 10^2 MN/m^2 yield stress, and 4.41 and 13.23 × 10^2 MN-m/m^3 local fracture toughness values.

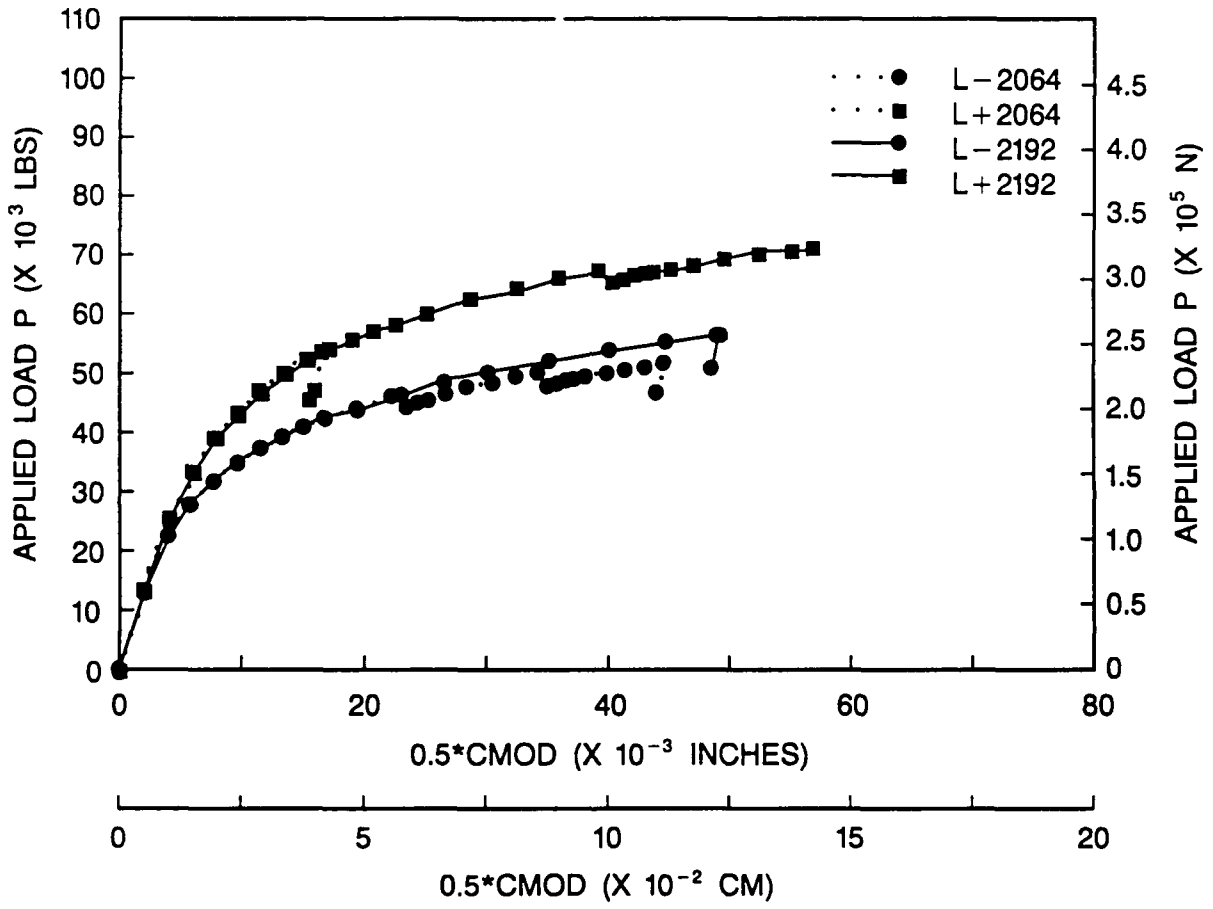

Fig. 12 — Applied load (P) versus crack mouth opening displacement (CMOD) for extreme combinations of strength and toughness. Long crack length, 5.79 and 8.55 × 10^2 MN/m^2 yield stress, and 4.41 and 13.23 × 10^2 MN-m/m^3 local fracture toughness values.

the low fracture toughness value includes only the pronounced strain hardening portion of the HY-100 nonlinear constitutive response. The moderate and high toughness values (i.e. Figures 2d and 2e) include both the pronounced and weak strain hardening portions of the HY-100 nonlinear constitutive response. The moderate and high toughness materials are apparently able to sustain the additional dissipated energy without a significant increase in elastic energy associated with this dissipation. The local elastic energy is also distributed in a more uniform manner over regions of large effective plastic strain. This apparently allows for more distributed local loading and unloading associated with crack growth.

Each simulation was planned to run for sixty load increments. Since the debonding sequence was not specified a priori and a range of material parameters were used, the amount of crack growth varied considerably. Crack growth for long and short crack length simulations are given in Tables 3 and 4, respectively. In several instances, combinations of material parameters, geometry, load and mesh were unable to maintain convergence with further loading or debonding at some point in the analysis. Material stress and strain limited convergence during crack growth was noted for some of the simulations. These occurrences, their cause and solution are discussed here.

For the case of high yield stress, elastic stresses increase with yield stress for a given value of equivalent plastic strain. The crack growth increments produce simultaneous global unloading and increased plastic deformation at the new crack tip. The global elastic unloading which developed during an increment of crack growth produced large displacements. This reflected the decrease in specimen compliance associated with an increasing crack length and the shift of the crack tip plastic zone.

High toughness critical absorbed strain energy density values were also associated with increasing computational demands on the simulations. The relatively low slope of the material responses produces large plastic strains. The coupled effect of high toughness and low yield stress material response is capable of producing the largest strains. These strains became difficult to sustain in conjunction with the debonding for the longer crack simulations. Additional refinement in mesh size would facilitate additional debonding.

Yield Stress,		Local Fracture Toughness, x 10^2 MN-m/m^3		
x 10^2 MN/m^2		Low	Moderate	High
		4.41	8.83	13.23
High	8.55	4	-	3
Moderate	7.17	4	3	2
Low	5.79	3	-	2

Elements	a/a_0
1	1.17
2	1.33
3	1.50
4	1.67

Table 3 Number of elements sustaining crack growth for short crack length geometry

Yield Stress,		Local Fracture Toughness, x 10^2 MN-m/m^3		
x 10^2 MN/m^2		Low	Moderate	High
		4.41	8.83	13.23
High	8.55	1	-	2
Moderate	7.17	4	2	2
Low	5.79	3	-	1

Elements	a/a_0
1	1.09
2	1.18
3	1.27
4	1.36

Table 4 Number of elements sustaining crack growth for long crack length geometry

From each of these considerations, the following conclusions can be drawn. First, for simulations of relatively short length cracks sustaining significant crack growth, the global load versus displacement response was piecewise continuous with relatively minor discontinuities reflecting the discrete debonding process. Additional mesh refinement would further reduce these discontinuities by providing finer crack increments. This modification is not necessary, however, to assess the load versus displacement response of the specimen. Second, large strains associated with low yield stress and high local fracture toughness reached limits governed by the mesh size ahead of the crack tip utilized in this investigation. Additional mesh refinement would be necessary to sustain crack growth preceded by effective log plastic strains over 1.0. Third, the highest yield stress materials considered generated significant elastic displacements as a result of unloading which occured during debonding increments. In this case, additional mesh refinement would reduce the magnitude of unloading sustained by each debond increment.

It should be noted that many materials have lower yield stresses, sustain smaller strains and respond with a lower local fracture toughness than HY-100 or the parametric variations considered here. In view of the relative size of the computational resources allocated to any individual simulation, the ability to conduct analyses based on approaches such as those presented here are currently feasible and will continue to grow as improvements in computer technology continue to become available.

VI Summary

Parametric computational studies of stable crack growth in a modified compact tension specimen geometry were conducted. Computational modeling issues of crack growth prediction using a local fracture criterion were addressed using finite element analysis incorporating a debonding algorithm. The debonding algorithm utilized a user subroutine to assess local fracture at the crack tip and a nodal release scheme to produce crack growth. Crack growth was treated as a dependent variable of the analysis.

HY-100 steel material parameters were used as a basis for nonlinear constitutive response and local fracture toughness. Reduced and enhanced material yield strength and fracture toughness were examined to assess their relative effects on local fracture at the crack tip, the rate at which the crack stability is approached and the global nonlinearity produced by the combination of inelastic material response and crack growth. A comparison of constant yield strength and local fracture toughness simulations suggest that while stress and strain levels which a material can sustain are important, the manner in which these stress and strain levels are obtained through constitutive nonlinearity is equally important to specimen strength and crack growth response.

The combined influence of the material responses and the finite element model on solution convergence for this type of analysis was discussed. The relative influence of high elastic stresses and large plastic strain on both local and global unloading encountered during nodal release were noted.

The results of this study suggest that the capability to model and simulate stable crack growth in two dimensions using local fracture criteria is computationally accessible. The simulations conducted in this investigation, representing strong, ductile and fracture resistant alloys, encompass the computational modeling requirements of many materials currently in use. The capability to extend local fracture criteria and crack growth simulation into three dimensions will be realized as computational technology continues to evolve.

Acknowledgements - The authors wish to acknowledge the interest and contribution of Hibbitt, Karlsson and Sorensen, Inc. for the computational implementation of the debonding algorithm in the ABAQUS finite element program

References

[1] Light, M. F., Luxmoore, A. and Evans, W. T., "Prediction of Slow Crack Growth by a Finite Element Method," Int. J. Fracture, Vol. 11, pp 1045-1046, 1975.

[2] Light, M. F., Luxmoore, A. and Evans, W. T., "Some Further Results on Slow Crack Growth Prediction by a Finite Element Method," Int. J. Fracture, Vol. 12, pp 503-506, 1976.

[3] Hellan, K. and Lotsberg, I., "On Absolute Convergence of the Separation Work as Calculated by the Release of Nodes in a Finite Element Model," Int. J. Fracture,Vol 13, pp 539-543, 1977.

[4] Nakagaki, M., Chen, W. H. and Atluri, N., "A Finite Element Analysis of Stable Crack Growth-I," Elastic Plastic Fracture, ASTM STP 668, ASTM, Philadelphia, PA, pp 195-213, 1979.

[5] Shih, C. F., deLorenzi, H. G. and Andrews, H. R., "Studies on Crack Initiation and Stable Growth," Elastic-Plastic Fracture, ASTM STP 668, ASTM, Philadelphia, PA, pp 65-120, 1979.

[6] Sorensen, E. P., "A Numerical Investigation of Plane Strain Stable Crack Growth Under Small Scale Yielding Conditions," Elastic-Plastic Fracture, ASTM 668, ASTM, Philadelphia, PA, pp 151-174, 1979.

[7] Du, S. and Lee, J. D., "Finite Element Analysis of Slow Crack Growth," Engng. Fract. Mech., Vol. 16, pp 229-245, 1982.

[8] Du, S. and Lee, J. D., "Variations of Various Fracture Parameters During the Process of Subcritical Crack Growth," Engng. Fract. Mech., Vol. 17, pp 173-183, 1983.

[9] Carifo, J. E., Swedlow, J. L. and Cho, C. W., "Computation of Stable Crack Growth using the J-Integral," Frature Mechanics: Seventeenth Volume, ASTM STP 905, ASTM, Philadelphia, PA, pp 503-511, 1986.

[10] Hoff, R., Rubin, C. A. and Hahn, G. T., "A New Finite-Element Technique for Modelling Stable Crack Growth," Engng. Fract. Mech., Vol. 23, pp 105-118, 1986.

[11] Amar, E. and Pineau, A, "Application of a Local Approach to Brittle-Ductile Transition in a Low-Alloyed Steel," Nuc. Engng. Des , Vol. 105, pp 89-96, 1987.

[12] Aoki, S., Kishimoto, K., Yoshida, T. and Sakata, M., "A Finite Element Study of Near Tip Deformation of a Ductile Material under Mixed Mode Loading," J. Mech. Phys. Solids, Vol. 35, pp 431-344, 1987.

[13] Boone, T. J., Wawrzynek, P. A. and Ingraffea, A. R., "Finite Element Modelling of Fracture Propagation in Orthotropic Materials," Engng. Fract. Mech., Vol. 26 pp 185-201, 1987.

[14] Otsuka, A., Tohgo, K. and Okamato, Y., "Relationship Between Ductile Crack Initiation and Void Volume Fraction," Nuc. Engng. Des., Vol. 105, pp 89-96, 1987.

[15] Miyamoto, H., Kikuchi, M., Fujii, A. and Kubo, M., "Some Considerations of Mechanism of Ductile Fracture," Num. Meth. in Fract. Mech., Proc. Fourth Int. Conf., Pineridge Press, Swansea, 1987

[16] Narasimhan, R. and Rosakis, A. J., "Stable Crack Growth in Elastic-Plastic Solids Under Plane Stress Conditions: A Finite Element Study," Num. Meth. in Fract. Mech., Proc. Fourth Int. Conf., Pineridge Press, Swansea, 1987

[17] Shivakumar, K. N. and Crews, J. H. Jr., "Energy Dissipation Associated with Crack Extension in an Elastic-Plastic Material," Engng. Fract. Mech., Vol. 28, pp 318-330, 1987.

[18] DeGiorgi, V. G., Kirby, G. C. III and Jolles, M. I., "Analytical Prediction of Fracture Toughness in a Compact Specimen," Engng. Fract. Mech., (In Press).

[19] Kardomateas, G. A., "Finite Element Investigation of Plane Strain Asymmetric Fully Plastic Fracture," Comp. Struct., Vol. 30, pp 1147-1151, 1988.

[20] Zhang, D. Z. and Huang, X. D., "The Crack Initiation and Plastic Work," Eng. Fract. Mech., Vol. 29, pp 415-421, 1988.

[21] Shivakumar, K. N. and Newman, J. C., Jr., "Numerical Fracture Simulation of Bend Specimens Using a CTOD Criterion," Eng. Fract. Mech., Vol. 32, pp 203-210, 1989.

[22] Chaboche, J. L., "Continuum Damage Mechanics: Present State and Future Trends," Nucl. Eng. Des. Vol. 105, pp 19-33, 1987.

[23] Murakami, S., "Progress of Continuum Damage Mechanics," JSME Int. J., Vol 30, pp 701-710, 1987.

[24] Nquyen, Q. S., " Mechanical Modelling of Anelasticity," Revue Phys. Appl., Vol. 23, pp 325-330, 1988.

[25] Sarfarazi, M., "An Overview of the Constitutive Behavior of Crystalline Solids," Eng Fract. Mech., Vol. 31, pp 1035-1046, 1988.

[26] Matic, P., Kirby, G. C. III and Jolles, M. I., "The Relation of Tensile Specimen Size and Geometry Effects to Unique Constitutive Parameters for Ductile Materials," Proc. R. Soc. London A 417, pp 309-333, 1988.

[27] Hibbitt, Karlsson, and Sorensen, Inc., "ABAQUS Theory Manual," Providence: Hibbitt, Karlsson and Sorensen, Inc., 1987a.

[28] Harvey, D. P. II and Jolles, M. I., "Correlations between Micromechanical Features and Material Toughness in HY-100 Steel," J. Mater. Eng., Vol. 10, pp 267-272, 1988.

[29] Hibbitt, Karlsson, and Sorensen, Inc., "ABAQUS User's Manual," Providence: Hibbitt, Karlsson and Sorensen, Inc., 1987b.